that harmonic operation permits the upper frequency range of fabrication to be extended for most dispersive-filter designs [4].

In view of the wide utility of large TB dispersive filters having high compression ratios and the degree of success in present development efforts, the outlook is extremely bright for continued progress in the field of acoustic surface-wave dispersive filters.

Acknowledgment

The authors wish to thank R. L. Lanphar for his assistance in the computational work and W. K. Masenten for his critical reading of the manuscript.

References

[1] J. R. Klauder, A. C. Price, S. Darlington, and W. J. Albersheim, "The theory and design of chirp radars," *Bell Syst. Tech. J.*, vol. 34, pp. 745–808, July 1960.
[2] W. R. Smith, H. M. Gerard, and W. R. Jones, "Analysis and design of dispersive interdigital surface-wave transducers," *IEEE Trans. Microwave Theory Tech.*, vol. MTT-20, pp. 458–471, July 1972.
[3] R. H. Tancrell and M. G. Holland, "Acoustic surface wave filters," *Proc. IEEE*, vol. 59, pp. 393–409, Mar. 1971.
[4] T. W. Bristol, W. R. Jones, G. W. Judd, and W. R. Smith, "Further applications of double electrodes in acoustic surface wave device design," presented at the 1972 IEEE G-MTT Int. Microwave Symp.
[5] E. K. Sittig and G. A. Coquin, "Filters and dispersive delay lines using repetitively mismatched ultrasonic transmission lines," *IEEE Trans. Sonics Ultrason.*, vol. SU-15, pp. 111–119, Apr. 1968.
[6] W. R. Smith, *et al.*, "Analysis of interdigital surface wave transducers by use of an equivalent circuit model," *IEEE Trans. Microwave Theory Tech.*, vol. MTT-17, pp. 856–864, Nov. 1969.
[7] M. K. Stelter, "Chrome etching and relief deposition," *J. Photochem. Etching*, vol. 1, pp. 4–6, Dec. 1966.
[8] W. S. Jones, C. S. Hartman, and T. D. Sturdivant, "Second order effects in surface wave devices," *IEEE Trans. Sonics Ultrason.*, SU-19, pp. 368–377, July 1972.
[9] C. E. Cook and M. Bernfeld, *Radar Signals*. New York: Academic Press, Inc., 1967.
[10] J. J. Campbell and W. R. Jones, "A method for estimating optimal crystal cuts and propagation directions for excitation of piezoelectric surface waves," *IEEE Trans. Sonics Ultrason.*, vol. SU-15, pp. 209–217, Oct. 1968.
[11] T. R. O'Meara, "The synthesis of 'band pass' all-pass time delay networks with graphical approximation techniques," Hughes Res. Lab., Malibu, Calif., Rep. 114, 1962.
[12] J. D. Maines, E. G. S. Paige, A. F. Saunders, and A. S. Young, "Simple technique for the accurate determination of delay-time variations in acoustic-surface-wave structures," *Electron. Lett.*, vol. 5, pp. 678–680, Dec. 1969.
[13] H. I. Smith, F. J. Bachner, and N. Efremow, "A high-yield photolithographic technique for surface wave devices," *J. Electrochem. Soc.*, vol. 118, pp. 821–825, May 1971.
[14] R. D. Haggarty, L. A. Hart, and G. C. O'Leary, "A 10,000:1 pulse compression filter using a tapped delay line linear filter synthesis technique," in *EASCON Rec.*, pp. 306–314, 1968.
[15] T. M. Reeder and W. R. Sperry, "Broad-band coupling to high-Q resonant loads," *IEEE Trans. Microwave Theory Tech.*, vol. MTT-20, pp. 453–458, July 1972.
[16] H. Urkowitz, "Ambiguity and resolution," in *Modern Radar*, R. S. Berkowitz, Ed. New York: Wiley, 1965, pp. 197–203.

The IMCON Pulse Compression Filter and its Applications

TOM A. MARTIN

Invited Paper

***Abstract*—The IMCON is a reflection-mode dispersive delay line capable of high performance in large time–bandwidth product pulse compression systems. As developed in this paper, the unique characteristics of the IMCON are obtained by reflection from a double grating array that is applied to the surface of a strip. Current models of the device have center frequencies in the 4–30-MHz range with bandwidth up to 15 MHz, dispersion to 320 μs, time sidelobes on the order of −40 dB (with equalization), and other spurious signals at least 70 dB below the compressed output.**

The characteristics of IMCON operation are developed from a consideration of the device's transfer function. In particular, the IMCON's high linearity and low sensitivity to fabrication and propagation problems are shown to be due to a unique error rejection effect. By comparison, the error rejection characteristics of single grating and dispersive transducer devices are found to be inferior to the IMCON. Data derived from operating pulse compression systems are utilized to demonstrate the low time sidelobe and high time–bandwidth capability of the IMCON.

Manuscript received September 18, 1972; revised October 26, 1972.
The author is with Andersen Laboratories, Inc., Bloomfield, Conn. 06002.

I. Introduction

THE IMCON is a reflection-mode dispersive delay line capable of high performance in large time–bandwidth pulse compression systems [1]. It has evolved from a synthesis of three earlier dispersive delay-line technologies: the dispersive strip delay line, the perpendicular diffraction delay line, and the reflection grating device of Sittig and Coquin.

The dispersive strip delay line, described by Meeker [2], makes use of the naturally dispersive characteristics of the first symmetric Lamb mode in a thin strip of metal. Although

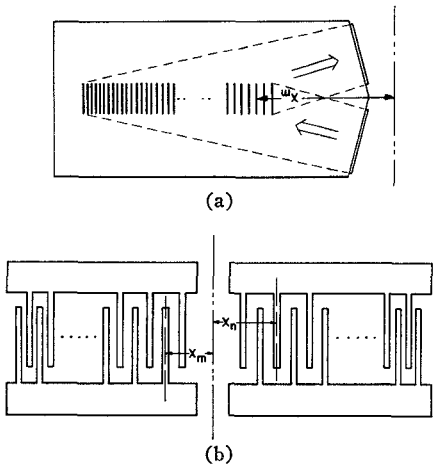

Fig. 1. "Single-summation" array configurations. (a) SCD. (b) Dispersive ID surface wave.

these devices have the advantage of simplicity and low cost, they are troubled by delay nonlinearities and insertion losses that grow rapidly with increasing time–bandwidth product. As a result, their maximum time–bandwidth product is limited to approximately 150. These devices have been built in great quantity over the past ten years, and a large body of fabrication technology and reliability experience has been accumulated.

A second dispersive delay-line technology that has aided the development of the IMCON is the perpendicular diffraction delay line (PDDL) described by Coquin and Tzu [3]. This device is commonly built on fused quartz with one transmitting array of acoustic line sources illuminating a similar receiving array on a perpendicular facet. The acoustic arrays are composed of hundreds or thousands of lines etched photolithographically into a standard bulk wave transducer. Although capable of broad bandwidths, the PDDL is limited in dispersion to approximately 35 μs because of quartz size limitations. The most important characteristic of the PDDL is its exceedingly low amplitude and phase ripple, which implies correspondingly low side lobes in a pulse compression system. This is achieved by the strong interaction of the mutually perpendicular transmitting and receiving arrays in which many different paths contribute to the response at a given delay time. This interaction causes a statistical reduction of fabrication-born amplitude and phase errors.

The grating reflection device of Sittig and Coquin [4] forms the third and most basic building block of the IMCON. Shown schematically in Fig. 1(a), the strip version of this device makes use of fabrication technologies developed with the strip dispersive delay line, combined with the grating technology used in the PDDL. The result is a delay line capable of large time–bandwidth products, but hindered by relatively strong amplitude and phase distortions, and therefore poor sidelobe performance.

The advantages and disadvantages of all three of these technologies led to the development of the IMCON [5]. The simplicity of the strip transmission-line configuration and the advantages of the planar reflection grating approach seemed to provide an expedient way to exploit the error rejection properties of the PDDL. This led to the conception of a configuration that would allow the interaction of two coplanar grating structures, as shown in Fig. 2.

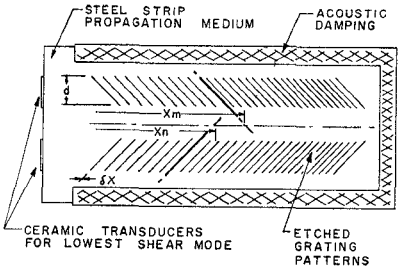

Fig. 2. IMCON configuration.

In Section II, the IMCON's transfer function is first approximated by a single-index summation and then evaluated in closed form in order to obtain device design criteria. Section III then uses the single-index summation form to compare the effects of fabrication errors on the IMCON and other dispersive array devices. The IMCON's general performance properties are discussed in Section IV, and specific pulse compression data are presented. Section V describes future IMCON capabilities.

II. IMCON Model

Physical Description: As shown in Fig. 2, the IMCON consists of a thin strip of solid material to which transducers are bonded and a grating pattern is photolithographically applied. The zero-order plate shear mode of propagation is utilized in the strip [6]. This mode is naturally nondispersive; that is, its phase velocity depends on neither frequency nor strip thickness. The strip is most commonly rolled spring steel, although fused quartz and aluminum are also useful in some circumstances. The strip must be kept slightly less than one wavelength thick in order to prevent undesirable interactions with other plate modes. The transducers are ferroelectric ceramics, such as PSN or PZT, bonded to the edge of the strip. They are poled in such a way to couple only to the shear modes of the strip. These transducers are noted for their high efficiency and broad bandwidth; 5-dB conversion loss per transducer over a 50-percent bandwidth is routinely achieved with simple impedance matching and less than 3 dB is possible with more complex matching. Both transducers are usually matched to 50 Ω.

The grating pattern is a herringbone-like structure with grating lines placed at 45° angles to the direction of signal propagation. The grating dimensions depend on the desired signal parameters, which are defined as follows: f_0 is the center frequency, Δf is the bandwidth, τ_0 is the center-frequency group delay, $\Delta\tau$ is the group delay dispersion, and $s=\Delta\tau/\Delta f$ is the dispersive slope. The first four of these may be chosen independently of one another. In the discussion that follows, the desired group delay response is given by $\tau(f)=sf$. The position of the nth grating line in either half pattern is given by

$$x_n = \sqrt{x_1^2 + 2c(n-1)}, \qquad n = 1, \cdots, N \qquad (1)$$

where $x_1=vs(f_0-\Delta f/2)/2$ is the position of the first line, $c=sv^2/2$ is the grating constant, and $N=f_0\Delta\tau/2+1$ is the number of lines in each half pattern. The optimum grating width d, which is dependent upon the signal parameters, will be discussed later. The phase velocity for the zero-order shear mode is denoted by v and is identical to the bulk shear velocity. For spring steel, $v=0.125$ in/μs$=3175$ m/s, which gives an incremental delay for the folded grating path of 16 μs/in.

Transfer Function: The IMCON's transfer function is developed here to enable response predictions, design parameter optimization, and evaluation of the effects of fabrication and propagation errors. The transfer function for the small reflection coefficient case (neglecting transduction, attenuation, and diffraction) can be written as

$$H(\omega) = \sum_{m,n=1}^{N} \rho^2 \eta^{(m+n-2)} \gamma_{mn} e^{-j\beta(x_m+x_n)} \tag{2}$$

where ρ and η are, respectively, the grating line reflection and transmission coefficients, which are assumed to be independent of the indices m and n. For shallow etched lines of constant width on thin strips, ρ is given by

$$\rho \cong 2\rho_0 \sin(\beta\delta x/2)$$

where $\rho_0 \approx -\delta h/2h$ is the step reflection coefficient, h is the strip thickness, δh is the etch depth, and δx is the grating line width. The function $\gamma_{mn} = \max[(1-|x_m-x_n|/d), 0]$ is the path aperture constriction for reflections from the mth and nth lines. $\beta = \omega/v$ is the shear wavenumber, where $\omega = 2\pi f$ is the angular frequency. x_m and x_n are the positions of the mth and nth grating lines.

Equation (2) is a conceptually simple transfer function representing the sum of individual nondispersive paths for all possible grating line pairs. The path reflecting from the mth grating line on one side of the IMCON and then the nth grating line on the other side includes two reflections, $m+n-2$ transmissions through grating lines in the path, an aperture constriction of γ_{mn}, and has total path length x_m+x_n.

Although straightforward, the expression of $H(\omega)$ in (2) is not useful for obtaining design or performance information. Direct numerical calculation is impractically long because N is typically several thousand.[1] However, it is possible to find a closed-form approximation to $H(\omega)$. The IMCON transfer-function evaluation is divided into two distinct phases: the first transforms the double summation into a single summation and the second evaluates the single summation in closed form.

The approximate single-summation form is derived in Appendix I using a transformation of indices, power series expansions, and an integral approximation:

$$H(\omega) = \sum_{l=2}^{2N} \rho^2 \eta^{(l-2)} \gamma_l e^{-j\beta 2x_{l/2}} \tag{3}$$

$$\gamma_l = \sqrt{4x_{l/2}{}^3/\beta c^2}\,\gamma(\sqrt{\beta d^2/4x_{l/2}}). \tag{4}$$

The function $\gamma(z_l)$ has been evaluated numerically and is shown in Fig. 3. Equation (3) is adequate for design estimations, but it should be remembered that the double summation is necessary for a complete representation. The significance of this distinction is explored later in the discussion of errors.

The second major step in the evaluation of $H(\omega)$ incorporates another index transformation and a stationary phase approximation, as described in Appendix II. The resulting

[1] A. MacMullen and D. Olsen of Technology Service Corp. have developed a practical recursive numerical technique for evaluating $H(\omega)$, including various types of random errors. Their results corroborate the analytical results of this paper for the case $\eta = 1-\rho_0^2$.

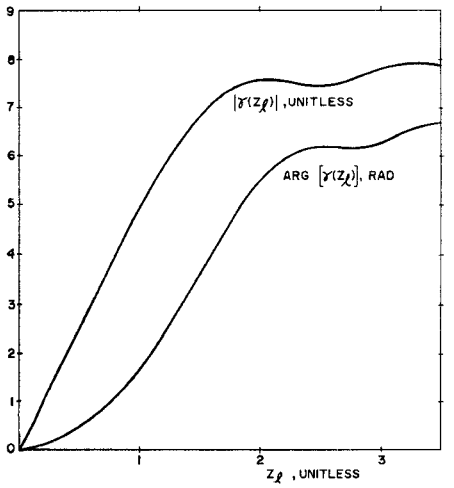

Fig. 3. Weighting function $\gamma(z_l)$ used in a single-summation representation of $H(\omega)$.

amplitude response is

$$|H(f)| = \rho^2 \eta^{s/2(f^2-(f_0-\Delta f/2)^2)} \frac{sf^2}{\sqrt{\pi}} \left| \gamma\left(\frac{d}{v}\sqrt{\frac{\pi}{s}}\right) \right| \tag{5}$$

and the group delay response is $\tau(f) = sf$, which is the desired response. Equation (5) can be used to establish design criteria for both the grating width d and the step reflection coefficient ρ_0. d is chosen so that $|\gamma(z_l)|$ in Fig. 3, and therefore $|H(f)|$, is near maximum while keeping d as small as possible (for fabrication and error rejection reasons). The following choice is usually made: $z_l = \sqrt{\pi}$, which implies $d = v\sqrt{s}$. ρ_0 can be chosen in several ways, one being such that $|H(f_0)| = 1$, with η set to unity. This implies that $-2\rho_0 = \delta h/h = 1/f_0\sqrt{s/2}$. For larger values of ρ_0, the small reflection coefficient hypothesis is violated and second-order effects become important.

III. Error Rejection Properties of the IMCON

Relationship Between Reflection Coefficient Errors and Transfer-Function Errors

It is possible to determine the effect of reflection coefficient errors on the IMCON's transfer function. Such errors are due to (for instance) incorrect grating line positions on the master grating, distortions in photolithography due to thermal or mechanical stresses, poor control of etching (or deposition) thickness and uniformity, or distorted wave propagation due to inhomogeneities in the propogation media.

For purpose of analysis, it is convenient to represent the reflection coefficient of each grating line as a complex Fourier series:

$$\rho_m = \rho(1 + \mathrm{E}_m) \tag{6}$$

where

$$\mathrm{E}_m = \sum_{p=-\infty}^{\infty} \epsilon_p e^{j2\pi pm/N}, \qquad |\mathrm{E}_m| \ll 1. \tag{7}$$

The Fourier components ϵ_p provide an approximate representation of all errors described in the previous paragraph and ρ is the nominal reflection coefficient described in (2). Make the

assumption that $\eta_m = \eta$ and substitute (6) into (2) to obtain

$$H(\omega) = \sum_{m,n=1}^{\infty} \rho^2(1 + E_{1m})(1 + E_{2n})\eta^{(m+n-2)}\gamma_{mn} \cdot e^{-j\beta(x_m+x_n)} \quad (8)$$

where E_{1m} and E_{2n} correspond to the two half gratings. Neglecting terms of second order in E yields

$$(1 + E_{1m})(1 + E_{2n}) \approx 1 + E_{1m} + E_{2n} = 1 + \sum_{p=-\infty}^{\infty} (\epsilon_{1p}e^{j2\pi pm/N} + \epsilon_{2p}e^{j2\pi pn/N}). \quad (9)$$

The application of (20), (22), and (23) to (8) and (9) gives

$$H(\omega) = \sum_{l=2}^{2N} \rho^2\eta^{(l-2)}\gamma_l \cdot \left[1 + \sum_{p=-\infty}^{\infty} (\epsilon_{1p}\mu_{lp} + \epsilon_{2p}\mu_{l(-p)})e^{j\pi pl/N}\right] \cdot e^{-j\beta 2x_{l/2}} \quad (10)$$

where γ_l is given in (4) and

$$\mu_{lp} = \gamma_l^{-1} \sum_{k=k_{l1}}^{k_{l2}} \frac{1}{2} \max\left[(1 - |kc/x_{l/2}|/d), 0\right] \cdot e^{j(\beta c^2k^2/4x_{l/2}{}^3 + \pi pk/N)}. \quad (11)$$

The quantity μ_{lp} was evaluated using integral approximation techniques identical to those of Appendix I; μ_{lp} is even in p and is, for the purpose of this discussion, independent of l. Consequently, we shall denote μ_{lp} by μ_p. Fig. 4 shows an upper bound of $|\mu_p|$, which is called the "error rejection factor," as a function of $|p|/\sqrt{\Delta\tau\Delta f}$.

Paired echo theory [1] can now be used to draw a direct relationship between the pth Fourier error coefficient and the pth sidelobe level in a pulse compression system. This error rejection property is one of the IMCON's most important features. It is the mechanism by which a host of fabrication and wave propagation problems are eliminated, and by which low pulse compression sidelobes are achieved. It is fortunate that the low Fourier index errors, which are not rejected, fall within the domain of distortions amenable to external electronic equalization—a technique that is well developed [1].

Effects of Errors on Other Devices: It is instructive to now find the effects of reflection coefficient errors on other types of devices.

The Sittig–Coquin device (SCD), shown in Fig. 1(a), has the same number of grating lines as the IMCON; however, all of these lines are now in a single grating and the line spacing is one half wavelength. The transfer function for this device is

$$H_{SC}(\omega) = \sum_{l=2}^{2N} \rho_1\eta_1{}^{(2l-2)}e^{-j\beta 2x_{l/2}} \quad (12)$$

which we shall compare with (3). If the relationships $\rho_1 = \rho^2$ and $\eta_1{}^2 = \eta$ are imposed on the reflection and transmission coefficients, then (12) can be written as

$$H_{SC}(\omega) = \sum_{l=2}^{2N} \rho^2\eta^{(l-2)}\gamma_l{}^{SC}e^{-j\beta 2x_{l/2}} \quad (13)$$

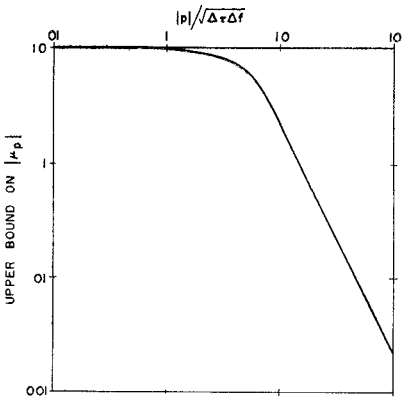

Fig. 4. Upper bound for the magnitude of the IMCON error rejection factor μ_p as a function of the normalized index $|p|/\sqrt{\Delta\tau\Delta f}$.

which is identical to (3) except that $\gamma_l{}^{SC}$ is now constant and equal to η. Thus (13) can be cast directly into the form of (5) using the techniques of Appendix II.

The SCD transfer function, with reflection coefficient errors, is found by substituting (6) into (13):

$$H_{SC}(\omega) = \sum_{l=2}^{2N} \rho^2\eta^{(l-2)}\gamma_l{}^{SC}\left[1 + \sum_{p=-\infty}^{\infty} \epsilon_p e^{j\pi pl/N}\right] \cdot e^{-j\beta 2x_{l/2}}. \quad (14)$$

Note that (14) is essentially identical to (10) except 1) there is only one ϵ_p instead of two because there is only one grating, and 2) most importantly, ϵ_p is *not* reduced by the error rejection factor μ_p shown in Fig. 4.

The dispersive interdigital (ID) array type of surface-wave delay line, shown in Fig. 1(b), can be described to the first order by

$$H_{ID}(\omega) = \sum_{m,n=2}^{2N} \gamma_m{}^{ID}\gamma_n{}^{ID}e^{-j\beta(x_{m/2}+x_{n/2})} \quad (15)$$

which can be rewritten [7] as

$$H_{ID}(\omega) = \left[\sum_{l=2}^{2N} \gamma_l{}^{ID}e^{-j\beta x_{l/2}}\right]^2. \quad (16)$$

Note that $H_{ID}(\omega)$ is essentially identical to a cascaded pair of (3) transfer functions with ρ and η set to unity. As such, the techniques of Appendix II will yield $H_{ID}(\omega)$ in closed form.

The addition of reflection coefficient errors (6) and (7) to (16) yields

$$H_{ID}(\omega) = \left[\sum_{l=2}^{2N} \gamma_l{}^{ID}\left[1 + \sum_{p=-\infty}^{\infty} \epsilon_p e^{j\pi pl/N}\right]e^{-j\beta x_{l/2}}\right]^2. \quad (17)$$

The comments made in the previous paragraphs apply equally to the ID surface wave device. Thus in spite of the fact that it has two gratings, the ID surface wave device acts as though it were two cascaded single grating devices, and as such *cannot* realize the benefits of the error rejection factor.

Experimental Evidence of Error Rejection: Fig. 5 shows an experimental comparison of SCD and IMCON performance. All parts of Fig. 5 were taken on the same amplitude and time scales and the intent is to illustrate the difference in response

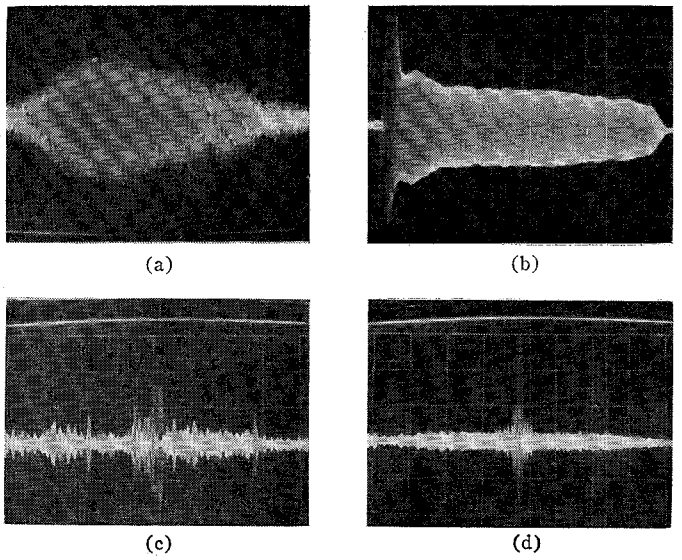

Fig. 5. Comparison of impulse responses and compressed pulse sidelobes for the SCD and IMCON. (a) SCD impulse response. (b) IMCON impulse response. (c) SCD compressed pulse. (d) IMCON compressed pulse. A reference exposure at −30 dB is included in (c) and (d). All time scales are 10 μs/div.

and sidelobe structure. Each line operates at 30 MHz in a recirculated pulse compression system with a bandwidth of 3 MHz and a dispersion of 50 μs. The impulse response of the IMCON shows a marked reduction in random errors over that of the SCD. The far-out sidelobe structure of the SCD shows sidelobe peaks of nearly 30 dB, while the far-out sidelobe structure of the IMCON shows better than 40-dB sidelobes. It should be noted that most of the far-out sidelobe energy in Fig. 5(d) is due to gating (i.e., Fresnel) sidelobes and does not represent delay-line distortion.

IV. IMCON Properties

Tabulated below are the principal properties of IMCON's fabricated from spring steel using photoetched grating patterns and ceramic transducers.

Dispersion: Dispersions of up to 320 μs are presently obtainable.

Bandwidth: The IMCON is basically a broad-band device, capable of up to an octave bandwidth.

Center Frequency: Center frequencies up to 30 MHz are obtainable. Above this, attenuation and nonuniform wave propagation problems are encountered. In addition, fabrication becomes difficult since the strip must be less than a wavelength thick.

Insertion Loss: The IMCON is a relatively low-loss device with that loss being attributable to four separate mechanisms in most designs. 1) Transducer loss, which typically amounts to 5 dB per transducer. 2) Reflection loss through the IMCON grating structure, which typically totals 10 dB. 3) Damping loss due to acoustic damping material applied between the two IMCON half gratings in order to flatten the amplitude response and/or further reject multiple transit responses. This is usually somewhere between 0 and 10 dB of loss. 4) Propagation loss in the steel that has been determined experimentally and is shown graphically in Fig. 6. Also shown for comparison purposes are the attenuation losses of glass and fused quartz, which are common delay-line materials.

Amplitude Flatness: The IMCON is often capable of ±0.5 dB amplitude ripple over up to an octave bandwidth due to a

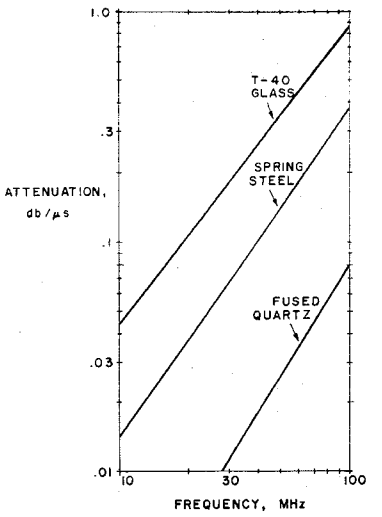

Fig. 6. Shear wave propagation attenuation for spring steel, T-40 glass, and fused quartz.

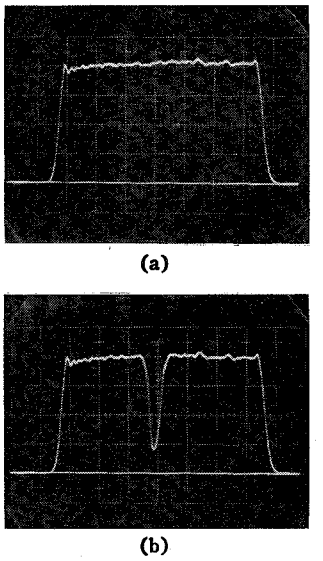

Fig. 7. Effect of acoustic damping between the IMCON gratings. Amplitude response is shown for (a) no damping and (b) localized damping.

unique fabricational control over the bandpass shape. As Fig. 2 shows, in the area between the two half grating patterns there is a one-to-one relationship between frequency and distance measured along the length of the gratings. Thus a localized application of acoustic damping material between those gratings will produce a localized dip in the impulse or frequency response of the IMCON. Fig. 7 shows the effect of a finger tip applied to the area between the two grating patterns. This means that acoustic damping materials can be used to easily shape the amplitude response of an IMCON without effecting its phase response. By the same token, it is possible to use techniques such as thin-mass loading films between the grating patterns to shape the phase response of an IMCON without effecting its amplitude response.

Spurious: The IMCON's spurious performance is excellent. Feed-through and multiple transit spurious can usually be held to −50 dB or better when measured with a CW burst. Furthermore, when the IMCON is used in a pulse compression receiver, such spurious are further decreased by the correlation gain. Other types of spurious associated with unwanted

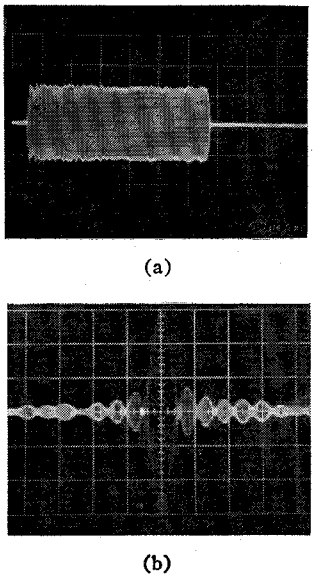

(a) (b)

Fig. 8. Type 7452. (a) Impulse response; 50 μs/div. (b) Compressed pulse; 0.2 μs/div.

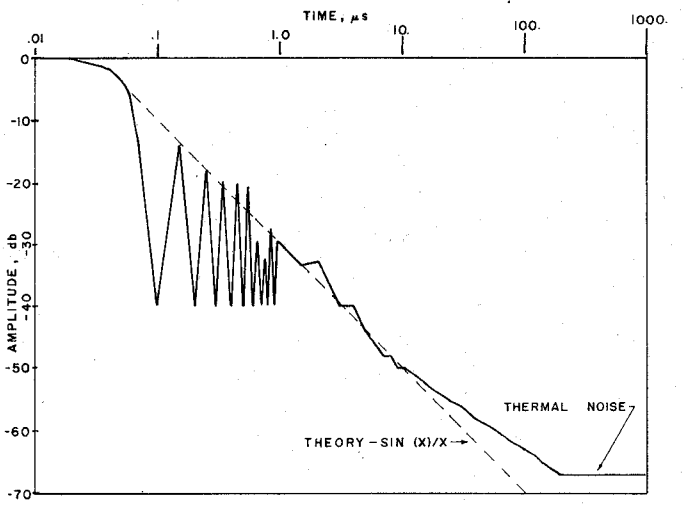

Fig. 9. Type 7452 compressed pulse; log–log representation of the right half of the pulse. Sidelobe details are plotted for $t<1$ μs. Sidelobe peaks only are plotted for $t>1$ μs. The theoretical sin $(x)/x$ response is shown for comparison.

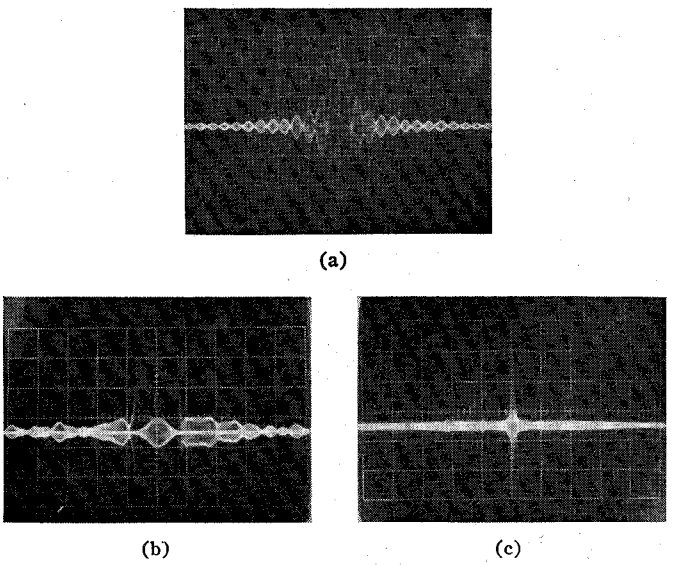

(a) (b) (c)

Fig. 10. Type 7743 compressed pulse. (a) Unweighted; 0.5 μs/div. (b) Weighted; 0.5 μs/div with −36.5-dB reference exposure. (c) Weighted; 50 μs/div with 1-div peak-to-peak on the vertical scale corresponding to −50 dB down from the peak response.

plate modes are very effectively rejected by the IMCON grating pattern. It can be shown that when the IMCON is properly designed these modes can never find their way to the output transducer, but are instead absorbed in the damping material around the perimeter of the IMCON [9].

Group Delay Response: The IMCON may be designed for either linear or nonlinear group delay responses as required by the application [1]. The great majority of applications call for linear FM responses, in which case deviations from a least-squares linear fit to the group delay data typically amounts to 0.05 percent of the dispersion. This means that a minimum amount or no phase equalization is required in order to achieve low sidelobes. It also means that the IMCON exhibits excellent Doppler performance. Compressed pulse degradations due to Doppler shifts will be limited by weighting filter mismatch [1], not delay-line nonlinearities.

Center-Frequency Delay: The center-frequency delay is a completely independent design parameter. It depends upon the distance chosen between the IMCON grating pattern and the transducers.

Slope: The algebraic sign of the dispersive slope is an independent design parameter.

Temperature Coefficient: The temperature coefficient of group delay is a function of the independent design parameters given above, and is therefore under the control of the delay-line designer. With this flexibility it is possible to build an IMCON with vanishing group delay temperature coefficient at midband, which implies output pulse position temperature invariance in a pulse compression system.

Size: The IMCON is small in size when compared to many of the possible alternate approaches such as lumped constant, dispersive strip line, tapered dispersive strip line, or PDDL. Preliminary results indicate also that the IMCON may be coiled to diameters of 1–2 in without degradation of performance. This means that even very long dispersions may be achieved in packages measuring only a few inches cubed.

IMCON Applications Data: Data on three representative IMCON pulse expansion/compression systems are presented below.

Type 7452: An unweighted pulse compression system was developed to demonstrate the feasibility of a system with very high correlation gain, i.e., very large time–bandwidth product. The system operates at 20 MHz with 10-MHz bandwidth and 250-μs dispersion, yielding a time–bandwidth product of 2500. The IMCON's in the system were gated down to the 10-MHz/250-μs parameters. The IMCON's were actually 12.5 MHz wide with 312.5-μs dispersion, giving them a time–bandwidth product of nearly 4000. The system's measured correlation gain was 33.5 dB, which is but 0.5 dB from ideal. Fig. 8(a) shows the impulse response of a type 7452 IMCON. The compressed pulse sidelobe structure is shown on both linear [Fig. 8(b)] and log–log (Fig. 9) scales. The significance of Fig. 9 lies in the near-theoretical sidelobe structure, especially at times far removed from the main response. It is seen that the sidelobe level decreases uniformly down to a "floor" of −67 dB, which is the receiver's output thermal noise level. This is in sharp distinction to "single grating" devices where a much higher sidelobe "floor" covers the entire correlation interval even for modest time–bandwidth products. [See Fig. 5(c).]

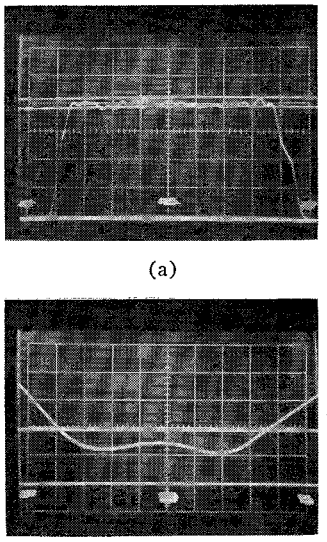

(a)

(b)

Fig. 11. Type 7759 responses. (a) Amplitude with −27.3- and −27.6-dB references. (b) VSWR with 1.5:1 reference. In both (a) and (b) the sweep rate is 1 MHz/div and the midscale corresponds to 15 MHz.

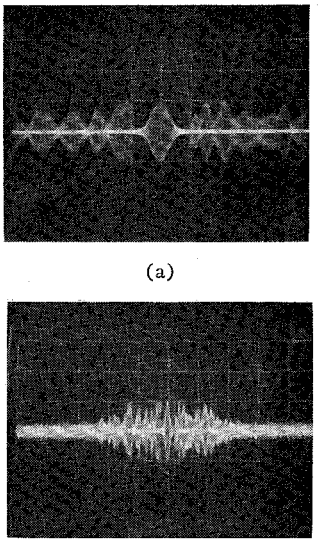

(a)

(b)

Fig. 12. Type 7759 weighted compressed pulses. (a) 0.5 μs/div. (b) 2 μs/div. Both (a) and (b) have −40-dB reference exposures.

Type 7743: A weighted pulse compression system was developed with a 1250 time–bandwidth product system. The system operated at 10 MHz with 5-MHz bandwidth and 250-μs dispersion and a Hamming weighting function was employed. Fig. 10 shows the unweighted system output with −13-dB sidelobes and the weighted system output. The weighted sidelobe level is −36.5 dB and the pulsewidth (−4 dB) is a near-theoretical 305 ns. All spurious are down at least 70 dB from the compressed pulse.

Type 7759: Another weighted pulse compression system was developed to demonstrate low sidelobes in a moderate (600) time–bandwidth product system. The system operated at 15 MHz with 6-MHz bandwidth and 100-μs dispersion and a Hamming weighting function was employed. Fig. 11 shows the amplitude and VSWR characteristics of a type 7759 IMCON. Fig. 12 shows the system output. The sidelobe level

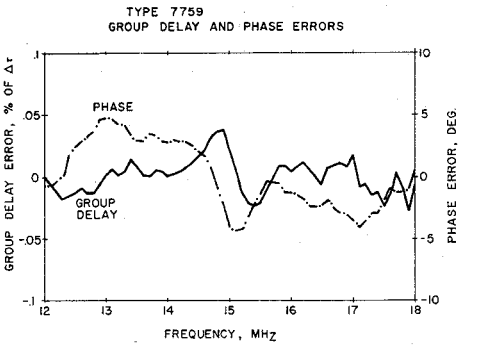

Fig. 13. Type 7759 group delay and phase errors.

is −40 dB and the pulsewidth (−4 dB) is a near-theoretical 260 ns. Note the rapid sidelobe decay as predicted by the error rejection factor. All spurious are down at least 80 dB from the compressed pulse. Fig. 13 shows the group delay and phase errors over the frequency band. These are the errors that remain after a least-squares fit (quadratic for phase, linear for group delay) has been subtracted from the data.

V. Future IMCON Capabilities

It is interesting to explore how the IMCON's capabilities might be expanded in the future. Several specific areas are identified and explored here.

Bandwidth: The IMCON's present limitation of 15-MHz bandwidth is the most serious limitation on its general usefulness. An extension of the bandwidth to 20 MHz is a possibility; however, an extension beyond that using strip techniques is not feasible for the reasons indicated in Section IV. A much more important route to wider bandwidth is the surface-wave IMCON, or reflective array compressor (RAC) [8], [9].

It is possible to implement the surface-wave IMCON on both piezoelectric and nonpiezoelectric substrates, which affords the following advantages at microwave bandwidths: the material can be chosen for its high velocity in order to alleviate photolithographic problems; it can be chosen for low attenuation; or it can be chosen for desirable crystal symmetries such as the cubic structure in which the velocity along and across the IMCON grating can be chosen equal so as to minimize the effects of misorientation. Surface-wave generation is more difficult with nonpiezoelectric substrates; however, several techniques exist and are rapidly developing toward greater efficiencies and/or bandwidths. These include the grating mode converter [10], [11], the thin-film overlay [12], the bonded planar substrate [13], and the high-efficiency wedge [14].

Dispersion: The steel IMCON's present maximum dispersion is 320 μs, due simply to photolithographic equipment limitations. Extension to 600 μs simply requires larger equipment. Extension to 1 ms would involve the development of either a folded pattern or photolithographic processing in sections.

Time–Bandwidth Product: It is the author's opinion that the −35-dB sidelobe IMCON system is limited in the time–bandwidth product to approximately 10 000. Based on extrapolation of IMCON performance for devices with several thousand time–bandwidth product, it is felt that the phase equalization problem, in addition to the problems of attenuation and velocity variations with temperatures, will become exceedingly difficult above 10 000.

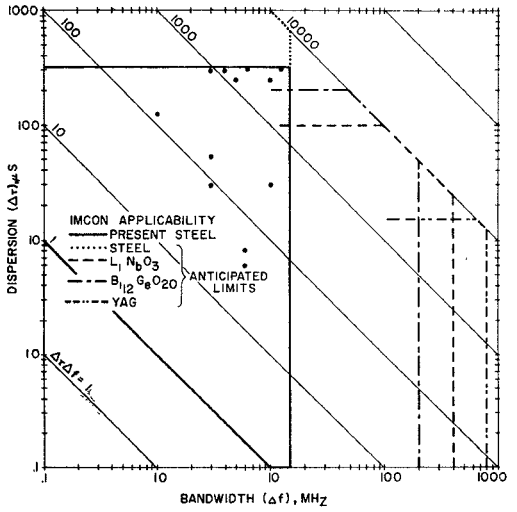

Fig. 14. Range of present and anticipated IMCON capabilities.

Linear FM Domain: A pictorial presentation of present and anticipated IMCON capabilities is given in Fig. 14. The solidly outlined area gives the present limits. The areas outlined otherwise give the projected range of applicability after the expenditure of varying amounts of development effort. The small circles represent the IMCON's built and the systems tested at Andersen Laboratories. Shown are the extended IMCON on steel strip and the surface-wave IMCON on LiN_bO_3, $Bi_{12}GeO_{20}$, and YAG. The upper-bandwidth limitation on the surface-wave IMCON is determined by 50-percent bandwidth and 1-μm linewidths, and the dispersion limits are established by present-day crystal growth capabilities.

VI. Conclusions

The IMCON and its properties have been described in detail. The IMCON on steel strip is well advanced in development and has demonstrated exceptional performance in high time–bandwidth applications. The development of the surface-wave IMCON is presently underway and will provide high performance broad-band devices. The future IMCON in its various forms will cover an exceptionally large expanse of the linear FM signal domain.

Appendix I

Single-Summation Index Approximation to the IMCON Transfer Function

The IMCON's transfer function is given by

$$H(\omega) = \sum_{m,n=1}^{N} \rho^2 \eta^{(m+n-2)} \gamma_{mn} e^{-j\beta(x_m+x_n)} \tag{18}$$

where

$$\gamma_{mn} = \max\left[(1 - |x_m - x_n|/d), 0\right]. \tag{19}$$

Define new indices l and k as

$$l = m + n \qquad k = m - n. \tag{20}$$

Substitution of (20) into (18) and (19) yields

$$H(\omega) = \sum_{l=2}^{2N} \rho^2 \eta^{(l-2)} \sum_{k=k_{l1}}^{k_{l2}} \gamma_{lk} e^{-j\beta x_{lk}} \tag{21}$$

where

$$\gamma_{lk} = \max\left[(1 - |\Delta x_{lk}|/d), 0\right]/2$$
$$x_{lk} = x_m + x_n = x_{(l+k)/2} + x_{(l-k)/2}$$
$$\Delta x_{lk} = x_m - x_n = x_{(l+k)/2} - x_{(l-k)/2}. \tag{22}$$

By performing power series expansions of (22) in k, it is possible to write

$$x_{lk} = 2x_{l/2} - c^2k^2/4x_{l/2}^3 + \cdots$$
$$\Delta x_{lk} = kc/x_{l/2} + \cdots. \tag{23}$$

Substitution of (23) into (21) and (22) yields

$$H(\omega) = \sum_{l=2}^{2N} \rho^2 \eta^{(l-2)} \gamma_l e^{-j\beta 2x_{l/2}} \tag{24}$$

where

$$\gamma_l = \sum_{k=k_{l1}}^{k_{l2}} \frac{1}{2} \max\left[(1 - |kc/x_{l/2}|/d), 0\right] \cdot e^{j\beta c^2k^2/4x_{l/2}^3}. \tag{25}$$

It is possible to approximate γ_l in closed form. First, neglect effects occurring only at the ends of the grating (i.e., $l \approx 2$ or $2N$) by setting

$$-k_{l1} = k_{l2} = k_l = dx_{l/2}/c. \tag{26}$$

Second, note that the terms in (25) are slowly changing and are of stationary phase at $k=0$. Then (25) can be approximated by the integral

$$\gamma_l = \sqrt{4x_{l/2}^3/\beta c^2}\, \gamma(z_l) \tag{27}$$

where

$$\gamma(z_l) = \int_0^{z_l} (1 - z/z_l) e^{jz^2} dz, \qquad z_l = \sqrt{\beta d^2/4x_{l/2}}. \tag{28}$$

The function $\gamma(z_l)$ is plotted in Fig. 3. Thus (24), (27), and (28) yield $H(\omega)$ in the desired approximate single-summation index form.

Appendix II

A Closed-Form Approximation for the IMCON Transfer Function

It is desired to find a closed-form approximation to

$$H(\omega) = \sum_{l=2}^{2N} \rho^2 \eta^{(l-2)} \sqrt{4x_{l/2}^3/\beta c^2}\, \gamma\left(\sqrt{\beta d^2/4x_{l/2}}\right) \cdot e^{-j\beta 2x_{l/2}}. \tag{29}$$

This will be accomplished via an index transformation and the principle of stationary phase.

At any given frequency $\omega = v\beta$, there is a specific group of lines in the grating which contribute most strongly to the IMCON's response. The line in the center of that group (call it line number n_0) most nearly satisfies the one wavelength path difference condition:

$$\beta 2(x_{n_0/2} - x_{(n_0-1)/2}) = \beta c/x_{n_0/2} \approx 2\pi. \tag{30}$$

As a notational aid, introduce the modified shear wave number $\tilde{\beta}$, which is almost equal to β and in addition exactly satisfies the one wavelength path difference condition

$$\tilde{\beta}c/x_{n_0/2} \equiv 2\pi. \tag{31}$$

Now introduce the index transformation

$$l = n + n_0 \tag{32}$$

and note that by substituting (31) and (32) into (1), $x_{l/2}$ can be written as

$$x_{l/2} = \sqrt{(c\tilde{\beta}/2\pi)^2 + cn}. \tag{33}$$

Substitution of (32) and (33) into (29) plus some simple manipulation of the exponent yields

$$H(\omega) = e^{-j\beta 2x_{n_0/2}} \sum_{n=2-n_0}^{2N-n_0} \rho^2 \eta^{(n+n_0-2)} \sqrt{4x_{(n+n_0)/2}{}^3/\beta c^2} \cdot \gamma(\sqrt{\beta d^2/4x_{(n+n_0)/2}})e^{j\phi_n} \tag{34}$$

where

$$\phi_n = -\beta 2x_{(n+n_0)/2} + \beta 2x_{n_0/2} + 2\pi n. \tag{35}$$

Note that the addition of $2\pi n$ to (35) does not affect (34), but it serves to cast (35) in a form that is stationary in n at $n=0$. This then implies that the summation in (34) can be approximated by an integral and evaluated using the principle of stationary phase. Further substitution of (31) into the stationary phase result finally yields

$$H(\omega) = \rho^2 \eta^{(c\beta^2/4\pi - x_1{}^2/c)} \sqrt{\frac{c^2\beta\tilde{\beta}^3}{4\pi^5}} \gamma\left(\sqrt{\frac{\pi d^2\beta}{2c\tilde{\beta}}}\right) \cdot e^{-j[c/2\pi(\beta^2-\tilde{\beta}^2)-\pi/4]}. \tag{36}$$

The group delay of (36) is given by

$$\tau(\omega) \equiv -\frac{d\phi}{d\omega} = \frac{1}{v}\frac{d}{d\beta}\left[\frac{c}{2\pi}(\beta^2 - \tilde{\beta}^2) - \frac{\pi}{4}\right] = c\beta/\pi v. \tag{37}$$

If we evaluate $|H(\omega)|$ only at those frequencies ω, for which $\beta = \tilde{\beta}$, we obtain

$$|H(\omega)| = \rho^2 \eta^{(c\beta^2/4\pi - x_1{}^2/c)} \frac{c\beta^2}{\sqrt{4\pi^5}} |\gamma(\sqrt{\pi d^2/2c})| \tag{38}$$

or, in terms of more familiar parameters,

$$|H(f)| = \rho^2 \eta^{s/2(f^2-(f_0-\Delta f/2)^2)} \frac{sf^2}{\sqrt{\pi}} \left|\gamma\left(\frac{d}{v}\sqrt{\frac{\pi}{s}}\right)\right| \tag{39}$$

and $\tau(f) = sf$,which is the desired linear FM group delay response.

Acknowledgment

The author and Andersen Laboratories wish to acknowledge the important support of the U.S. Navy and Raytheon Missile Systems Division in the development of the IMCON.

References

[1] C. E. Cook and M. Bernfeld, *Radar Signals*. New York: Academic, 1967.
[2] T. R. Meeker, "Dispersive ultrasonic delay lines using the first longitudinal mode in a strip," *IRE Trans. Ultrason. Eng.*, vol. UE-7, pp. 53–58, June 1960.
[3] G. A. Coquin and R. Tzu, "Theory and performance of perpendicular diffraction delay lines," *Proc. IEEE*, vol. 53, pp. 581–591, June 1965.
[4] E. K. Sittig and G. A. Coquin, "Filters and dispersive delay lines using repetitively mismatched ultrasonic transmission lines," *IEEE Trans. Sonics Ultrason.*, vol. SU-15, pp. 111–119, Apr. 1968.
[5] T. A. Martin, "A new dispersive delay line," presented at the 1970 IEEE Ultrasonic Symp., San Francisco, Calif., Oct. 21–23, 1970.
[6] A. H. Meitzler, "Ultrasonic delay lines using shear modes in strips," *IRE Trans. Ultrason. Eng.*, vol. UE-7, pp. 35–43, June 1960.
[7] R. H. Tancrell and M. G. Holland, "Acoustic surface wave filters," *Proc. IEEE*, vol. 59, pp. 393–409, Mar. 1971.
[8] R. C. Williamson and H. I. Smith, "Large timebandwidth product surface wave pulse compressor employing reflective gratings," *Electron. Lett.*, vol. 8, pp. 401–402, Aug. 10, 1972.
[9] ——, "The use of surface-elastic-wave reflection gratings in large time–bandwidth pulse compression filters," this issue, pp. 195–205.
[10] H. L. Bertoni, "Piezoelectric Rayleigh wave excitation by bulk wave scattering," *IEEE Trans. Microwave Theory Tech. (Special Issue on Microwave Acoustics)*, vol. MTT-17, pp. 873–882, Nov. 1969.
[11] R. F. Humphryes and E. A. Ash, "Acoustic bulk-surface-wave transducer," *Electron. Lett.*, vol. 5, May 1, 1969.
[12] R. Wagers *et al.*, "Improvements in zinc oxide overlay acoustic surface wave transducers," presented at the 1972 IEEE Ultrasonics Symp.
[13] M. T. Wauk and R. L. Zimmerman, "Bonded planar structures for efficient surface wave generation," presented at the 1972 IEEE Ultrasonics Symp.
[14] H. L. Bertoni and T. Tamir, "VHF-UHF surface wave studies—High efficiency wedge transducers," ECOM R & D Tech. Rep. ECOM-032801.